A General Functional Response of Cytotoxic T Lymphocyte-Mediated Killing of Target Cells

Saikrishna Gadhamsetty,[†*] Athanasius F. M. Marée,[‡] Joost B. Beltman,[†§] and Rob J. de Boer[†]
[†]Theoretical Biology and Bioinformatics, Utrecht University, Utrecht, the Netherlands; [‡]Department of Computational and Systems Biology, John Innes Centre, Norwich, United Kingdom; and [§]Division of Immunology, the Netherlands Cancer Institute, Amsterdam, the Netherlands

ABSTRACT Cytotoxic T lymphocytes (CTLs) kill virus-infected cells and tumor cells, and play a critical role in immune protection. Our knowledge of how the CTL killing efficiency varies with CTL and target cell numbers is limited. Here, we simulate a region of lymphoid tissue using a cellular Potts model to characterize the functional response of CTL killing of target cells, and find that the total killing rate saturates both with the CTL and the target cell densities. The relative saturation in CTL and target cell densities is determined by whether a CTL can kill multiple target cells at the same time, and whether a target cell can be killed by many CTLs together. We find that all the studied regimes can be well described by a double-saturation (DS) function with two different saturation constants. We show that this DS model can be mechanistically derived for the cases where target cells are killed by a single CTL. For the other cases, a biological interpretation of the parameters is still possible. Our results imply that this DS function can be used as a tool to predict the cellular interactions in cytotoxicity data.

INTRODUCTION

Cytotoxic T lymphocytes (CTLs) are critical to control and eliminate viral infections and tumors. Adoptive transfer of in vitro-activated CTLs has been shown to successfully induce tumor regression both in mice (1–3) and in humans (4). The rate at which a CTL kills target cells, as well as the variation of the killing rate when CTL and target cell densities change, is poorly characterized. Knowledge of these CTL killing efficiency parameters is important to estimate the critical CTL density required for sterilizing immunity to tumors and viral infections (5–8).

Analogous to the concept in ecology, the functional response of CTL-mediated killing is defined as the rate at which single CTLs kill targets, as a function of the CTL and the target cell densities (9,10). Multiplying the functional response with the density of CTLs gives the total killing rate, i.e., the total number of target cells killed per unit of time. Several studies examined the functional response of CTL-mediated killing (6,9–11). Using an analogy to the Michaelis-Menten model for enzyme-substrate kinetics, Borghans et al. (9) derived a functional response assuming that a CTL can kill one target cell at a time, and that a target cell can only be killed by one CTL. They found for such monogamous killing that the total killing rate should saturate to the same extent with an increase in either CTL or target cell densities. In recent in vitro studies, it was shown that a single CTL can polarize lytic granules toward multiple target cells simultaneously (12), and that multiple CTLs can interact with a single target cell at the same time (13). Thus, killing is probably not monogamous in all circumstances, and the above-mentioned functional response might not apply for regimes of killing that involve different cellular interactions.

A number of theoretical studies examined the functional response of CTL killing resulting from nonmonogamous killing regimes. In an early study, Merrill (10) extended the enzyme-substrate kinetics analogy by allowing multiple CTLs to bind and independently kill single target cells. He found that the total killing rate in this model saturates at lower target cell densities than CTL densities. Contrary to these results, Graw and Regoes (11) found that CTL killing efficiency does not saturate with increasing target cell densities in their agent-based model simulations, but saturates with increasing CTL densities. Adding to the confusion, Ganusov et al. (6) analyzed in vivo cytotoxicity data (14) and concluded that mass-action kinetics (i.e., no saturation) describe the CTL-mediated killing well. Taken together, it remains unclear how the CTL killing rates vary with CTL and target cell densities, and why we observe mass-action kinetics in some studies (6) and saturation in CTLs and/or targets in others (9–11).

In this study, we examine whether the differences in the functional responses of the different studies can be due to differences in the underlying CTL-target cell interactions. To address this question, we first create simulated data on well-defined killing regimes that differ in the allowed CTL-target cell interactions. For this purpose, we perform cellular Potts model (CPM) (15,16) simulations of a densely packed cellular environment (like in a lymph node or spleen). Next, for each of the simulated killing regimes, we examine whether a functional response can be mechanistically derived. Strikingly, we find that the total killing rate for all the killing regimes can be unified into a double-saturation (DS) function with two saturation constants, one for the target cells and another for the CTLs. The saturation

Submitted August 6, 2013, and accepted for publication January 29, 2014.

*Correspondence: s.gadhamsetty@uu.nl

Joost B. Beltman and Rob J. de Boer contributed equally to this article.

Editor: Leah Edelstein-Keshet.

0006-3495/14/04/1780/12 $2.00

http://dx.doi.org/10.1016/j.bpj.2014.01.048

constants for the CTLs and the target cells turn out to depend on the killing regime, and can hence be used to infer the cellular interactions that underlie in vivo and in vitro cytotoxicity assay data.

MATERIALS AND METHODS

Cellular Potts model

We simulate a region of a spleen or a lymph node using the two-dimensional CPM formalism. Similar to our previous studies (17,18), we consider a field representing the T-cell zone of a lymph node, which is composed of fibroblastic reticular cells (19) forming a reticular network (RN; ≈17% of the field), B cells as target cells (≈39%), and CTLs (≈39%), and let the rest of the field (≈5%) be extracellular matrix (ECM). After the initialization of the RN, both B cells and CTLs are initialized at empty random positions as a square of 9 μm^2, which subsequently grow to their target area of 44 μm^2, corresponding to a diameter of almost 8 μm (5). Changes in the cell configuration and movements of the cells occur due to minimization of the surface energy of the cells. At each time step, all pixels are considered for extension into a random neighboring site, and the change in surface energy due to an extension is calculated by the difference in Hamiltonians H of two configurations. The Hamiltonian is given by

$$H = \sum_{ij}\sum_{i'j'} J_{\tau(\sigma_{ij}),\tau(\sigma_{i'j'})}\left(1-\delta_{\sigma_{ij},\sigma_{i'j'}}\right) + \sum_{\sigma}\lambda\left(a_\sigma - A_{\tau(\sigma)}\right)^2, \quad (1)$$

where $J_{\tau(\sigma_{ij}),\tau(\sigma_{i'j'})}$ is the surface energy associated between a cell site (of state $\sigma_{i,j}$ and cell type $\tau(\sigma_{i,j})$) and the neighboring lattice site (of state $\sigma_{i',j'}$ and cell type $\tau(\sigma_{i',j'})$), λ is the inelasticity, δ is the Kronecker delta, a_σ is the actual area of the cell σ, and $A_{\tau(\sigma)}$ is the target area of cells of type $\tau(\sigma)$. The first term in Eq. 1 represents the sum of all surface energies, and the second term is an area constraint applied to maintain the size of the cells close to their target area. The probability that a lattice site is copied into the neighboring site obeys a Boltzmann equation, i.e., is 1 if $\Delta H < 0$, and $e^{-(\Delta H)/D}$ otherwise, where D represents the membrane fluctuation amplitude of cells. The entire model is implemented in the C programming language.

Motility of cells in the simulations

Naïve T and B cells in lymph nodes migrate in a consistent direction for several minutes, but exhibit no preference for directional migration in the long term, i.e., they perform a persistent random walk (20,21). Previously, we showed that a self-adjusting motility of T cells is sufficient to explain these dynamical properties of T cells in lymph nodes (17,18), and we here adopt the same algorithm. Briefly, the extensions of a lattice site along a target direction are made more likely than in other directions by extending ΔH for B cells and CTLs as

$$\Delta H = -\mu\cos(\alpha), \quad (2)$$

where μ is the directional propensity of cells, and α is the angle between the target direction and the direction of the considered displacement. At the start of the simulation, the target direction of cells is assigned randomly from a uniform distribution of $[-\pi, \pi]$, and it is asynchronously updated thereafter every 180 s based on its direction of recent migration. Immotile cells tend to be circular, whereas migrating cells are slightly elongated with an extended tail.

For the employed model parameters (described below), we find mean speeds of simulated CTLs and target cells of ~9.5 μm/min and 5.6 μm/min, respectively (representative speed profiles are shown in Fig. S1, *A–D*, in the Supporting Material). Using Fuerth's equation from Parkhurst and Saltzman (22), the motility coefficients of CTLs and B cells are estimated to be 66.3 μm^2/min and 25.9 μm^2/min, respectively (see Fig. S1 *E*), which are close to experimental findings (20,21,23). The mean-square displacement (see Fig. S1 *E*) confirms that the target cells and CTLs in our model roughly perform persistent random walks (17,20,24).

Killing algorithm

When a CTL and a target cell come into contact, they form a conjugate based on the rules of the killing regime (see Fig. S4 for algorithms of simulations). To keep cells in a conjugate together, we upregulate the adhesion between a CTL and its target immediately upon conjugate formation by decreasing the surface tension for these cells by $\gamma_{\text{adhesion}} = 60$. Thus, the effective surface tension between CTLs and targets in a conjugate γ_{conj} becomes $\gamma_{\text{CTL,tgt}} - \gamma_{\text{adhesion}}$. In addition to the upregulation of adhesion, we stop the active migration of both CTLs and targets in conjugates by setting the directional propensities μ of all conjugated cells to zero. Cells in a conjugate have a flattened interface zone due to the strong adhesion. Unless otherwise mentioned, we do not restrict the number of binding sites on CTLs and target cells, but the finite surface area of the cells naturally limits the maximum number of synapses that cells can form.

We perform simulations for four well-defined killing regimes: monogamous, joint, simultaneous, and mixed killing (Fig. 1 *A*). For monogamous killing, conjugates of only one CTL and one target cell are allowed to occur, whereas conjugates of any number of CTLs and target cells can be formed during mixed killing. In the joint killing regime, multiple CTLs are allowed to bind and jointly kill a target cell. Conversely, multiple targets can be killed by a single CTL in the simultaneous killing regime. Conjugates are followed throughout the simulation to count the duration of contact for all target cells in conjugates. For monogamous and simultaneous regimes, target cells are killed if their duration of contact with a CTL reaches the kill time, t_D. With respect to simultaneous killing, we considered CTLs to be able to kill multiple target cells all with the same kill time (each in t_D minutes), i.e., killing of individual targets does not slow down when a CTL kills multiple targets at the same time. We chose this simplest case due to the lack of experimental data concerning such changes in t_D. For the other two types of killing regimes (i.e., joint and mixed), we consider the killing rate of a target cell to be proportional to the number of CTLs bound to it, which is achieved by keeping track of the cumulative contact duration with all conjugated CTLs of a target. This implies that the time required to kill a target cell decreases linearly with the number of CTLs in a conjugate (e.g., two CTLs bound to a target would kill it in $t_D/2$ min, i.e., half the time required for single CTL to kill a target cell).

When the duration of contact for target cells in a conjugate reaches the kill time t_D, the target cell disappears in a few seconds (by setting its target area to -1 μm^2), and the CTL resumes its migration, if it is not conjugated to any other target cell. In all our simulations, CTLs can also serially kill any number of targets, i.e., CTLs require no re-arming time required between killing two consecutive targets. To maintain a constant target cell density in the field throughout the simulation, we introduce a new target cell at a random position as soon as the area of the killed cell has reached zero. To prevent new target cells from being created inside another cell, this randomly chosen point for introducing a target cell is required to be either in the ECM, or at the membrane between two cells. If conjugates break despite a strong adhesion preference, target cells remember the elapsed contact duration, i.e., upon renewed contact with the same or another CTL the kill signal accrues on the existing signal. After breakup of a conjugate, the CTL and the target resume their migration in the field if they are not conjugated to other cells.

To speed up the approach to steady state, CTLs are allowed to form conjugates (yet do not kill target cells) during an initialization period of 4 min. At the end of this initialization period, we draw a random number from a uniform distribution of (0 min, t_D min), to represent the time already elapsed in the conjugate. Conjugate formation during the initialization

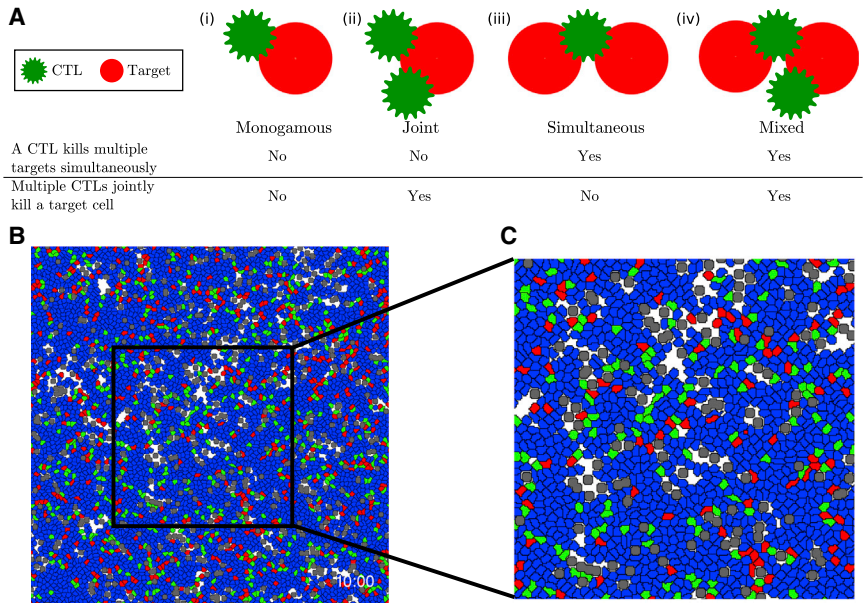

FIGURE 1 Illustration of the model. (*A*) Killing regimes. (*B*) Snapshot of a two-dimensional simulation. (*C*) Magnified view of a region of the field. (*Green*) CTLs; (*red*) target cells; (*gray*) reticular network. (*Blue*) Nonspecific target cells and CTLs. Snapshots shown in panels *B* and *C* are from simulations in the absence of killing with $\overline{E} = 500$ cells and $\overline{T} = 500$ cells. To see this figure in color, go online.

period, together with elapsed conjugate time assignment, results in a rapid approach to a quasi steady state (QSS) of killing dynamics, which is characterized by a constant number of conjugates during our simulations. We discard the initialization period in all analysis and plots. Following initialization we run each simulation for 600 min, i.e., 40 times the kill time t_D. To maintain similar migration properties at different frequencies of CTLs and target cells, we vary the number of antigen-bearing target cells, $\overline{T}$, and cognate CTLs, $\overline{E}$, while keeping the total number of T and B cells in the field constant. To make sure that the measured killing occurs at QSS, the number of cells killed is counted over the last 75 min of the simulation, and is averaged over six independent simulations for all CTL and target cell densities. Our analysis with six independent simulations resulted in a robust data set with little variability, as can be appreciated from the very low standard deviations (e.g., see Figs. 3–5, later in article). Each simulation took ~3 h of CPU time on a single Intel Xeon processor, 3.33 GHz, with 48 GB of memory.

Default model parameters

All the simulations are performed using the parameters described below (see Table 1 for a summary of the simulation parameters). We consider a two-dimensional torus of 500 × 500 pixels, where the length of each lattice site equals 1 μm. One time step in the simulation (i.e., attempting to update all the lattice sites) corresponds to 1 s in real-time. CPM is a phenomenological model (15,16), and its parameters have no biophysical meaning. We tuned CPM parameters such that the simulations capture in vivo migration properties of CTLs and B cells, a fraction of which are target cells. The surface energies J and the surface tensions γ are chosen such that the noncognate interactions between any pair of cells (including the RN) are neutral (see Table 2), i.e., there is no preferential adhesion. Other default parameters used in the simulations: $t_D = 15$ min (11,20), $\mu_{CTL} = 450$ for CTLs, $\mu_{tgt} = 220$ for targets, $\lambda = 200$, and $D = 6$.

Nonlinear regression (or fit) to the data

All the regression analyses of models to the data from simulations are performed using the function *nlinfit* in MATLAB (The MathWorks, Natick, MA), which uses the Levenberg-Marquardt algorithm. Log-transformed numbers of cells killed were used for all the regressions to prevent skewing of the fit to the killing observed at high CTL and target cell densities.

RESULTS

Cellular Potts model simulations

To determine the killing efficiency for different killing regimes, a CPM of simulated CTL and target cell (B cells in our case) migration in the T cell zone of a lymphoid tissue was constructed. The CPM is a grid-based model, in which each biological cell consists of multiple lattice sites (see Materials and Methods for details). Similar to our previous work on the migration of T cells and their interactions with dendritic cells (17,18), we consider a finite, wrapped two-dimensional space. Spleen and lymph nodes have a complex topology and constitute different cell types, but we consider for simplicity a space filled with static elements representing the fibroblastic RN that is present in lymph nodes ($\approx$17% of the space), 2250 CTLs, and 2250 target cells (representative snapshots of simulations are shown in Fig. 1, *B* and *C*). Note that the field is densely packed

TABLE 1 Summary of simulation parameters used

Parameter	Symbol	Value used
Time required to kill a target	t_D	15 min (11,20)
Inelasticity of the cells	λ	200
Membrane fluctuation amplitude of cells	D	6
Directional propensity of CTLs	μ_{CTL}	450
Directional propensity of targets	μ_{tgt}	220
Target direction update interval	—	3 min
Number of static elements representing RN	—	1050
Diameter of static elements	—	8 μm
Total number of CTLs	—	2250
Total number of target cells	—	2250
Target area of CTLs and target cells	A	44 μm^2

Parameters are chosen such that the simulated CTLs and B cells recapitulate migration properties observed in vivo. Surface energy parameters are mentioned in Table 2.

TABLE 2 Default surface energies and surface tensions used in the simulations

	ECM	RN	CTL	Target (tgt)
ECM	$J_{ECM,ECM} = 0$	$\gamma_{ECM,RN} = 0$	$\gamma_{ECM,CIL} = 0$	$\gamma_{ECM,tgt} = 0$
RN	$J_{RN,ECM} = 0$	$J_{RN,RN} = 0$	$\gamma_{RN,CIL} = 150$	$\gamma_{RN,tgt} = 150$
CTL	$J_{CIL,ECM} = 150$	$J_{CIL,RN} = 300$	$J_{CTL,CTL} = 0$	$\gamma_{CIL,tgt} = 0$
tgt	$J_{tgt,ECM} = 150$	$J_{tgt,RN} = 300$	$J_{tgt,CTL} = 300$	$J_{tgt,tgt} = 300$

Surface energies are represented by J, and γ are the surface tensions in arbitrary units.

with RN, CTLs, and targets, and only ~5% of the space is ECM. We perform simulations with different numbers of antigen-bearing target cells and their cognate CTLs, while keeping the total number of CTLs and target cells constant (2250 cells each). All the CTLs and targets exhibit the same migration properties, irrespective of their antigen status. This approach restricts confounding effects of different motility patterns that may arise when antigen-specific cell numbers are varied. CTLs and target cells perform a persistent random walk according to a set of well-defined migration rules (see Materials and Methods for details), which result in a realistic cell migration (see Fig. S1) and cellular interactions (17,18).

Recent imaging studies suggested that multiple CTLs can jointly kill a target, and one CTL can kill multiple targets simultaneously (12,13). To identify a general functional response, we therefore perform simulations for four different killing regimes: monogamous, joint, simultaneous, and mixed killing (Fig. 1 *A*; note that this nomenclature is chosen from the viewpoint of the CTL). In the monogamous killing regime, conjugates of just one CTL and one target cell are allowed to form. In the mixed killing regime, a CTL can induce death of multiple target cells simultaneously, and a target cell can be killed by multiple CTLs. Joint and simultaneous killing regimes are intermediates between monogamous and mixed. For joint killing, a CTL can kill only a single target cell at a time, but a target cell can be killed by many CTLs acting together (similar to the case that Merrill (10) considered). Conversely, in the simultaneous regime, a CTL can induce death of multiple target cells simultaneously, but a target cell can be killed by a single CTL only. It is unknown how the killing time t_D varies with the number of CTLs and target cells in a conjugate. For simplicity, we therefore make the killing rate proportional to the number of synapses formed per target cell, and the rate at which CTLs kill individual targets does not decline with the number of synapses they have with target cells. Note that rather than explicitly modeling the binding sites (10), the finite surface area of CTLs and target cells in the CPM naturally restricts the maximum number of synapses that cells can form, unless otherwise specified.

A killing time t_D of 15 min is used in all the simulations. After an initial transient of 4 min, the number of cells killed over 5-min intervals, and the number of synapses that target cells have with CTLs, are recorded every 5 min (Fig. 2) to assess QSS. Because we want to fit mathematical models to our artificial data after the system has reached QSS, we only use the number of cells killed during the final 75 min of the simulation, which was sufficient to approach to QSS for all regimes. For a given CTL and target cell density, the total number of synapses with targets comprises the lowest for the monogamous killing regime (Fig. 2 *A*), because only one CTL can be in synapse with a target cell. Another factor that likely plays a role in the rather subtle differences among joint, simultaneous, and mixed killing is that, in our simulations, CTLs migrate faster than targets, and conjugates do not actively migrate. In the mixed killing regime, we observe more synapses than there are target cells because multicellular conjugates of several CTLs and several targets can occur (Fig. 2 *A*). Because killing takes 15 min in the monogamous killing case, and the number of cells killed is recorded over 5-min intervals, the number of cells killed is approximately one-third of the number of conjugates at QSS (Fig. 2 *B*).

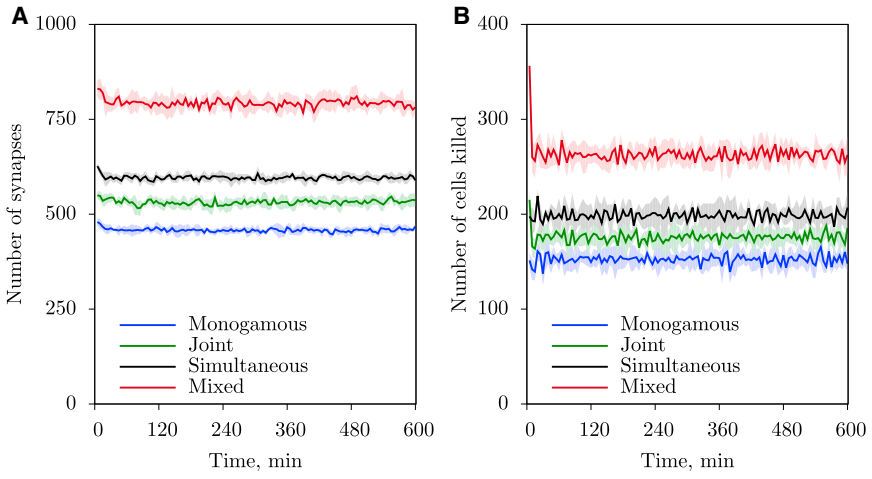

FIGURE 2 The total number of synapses with target cells (*A*) and the number of cells killed (*B*) over 5-min intervals during simulations with $\overline{E} = 750$ cells and $\overline{T} = 750$ cells for the four killing regimes. (*Solid lines*) Average from six independent simulations; (*shaded regions*) standard deviations over these six observations. The dynamics of conjugates and cells killed during the initialization period are not shown (i.e., time $t = 0$ denotes the time point after this initialization. The dynamics of conjugates and cells killed does not exhibit any correlation with time (Spearman's correlation $|\rho_S| < 0.09$, $P > 0.23$). To see this figure in color, go online.

Monogamous killing

In our monogamous killing simulations (see Movie S1 in the Supporting Material for a representative simulation), CTLs and targets form complexes that dissociate after a contact duration $t_D = 15$ min into a free CTL and a dying target cell (see Fig. S4 for a simplified simulation algorithm). For this scenario, Borghans et al. (9) followed the Michaelis-Menten analogy to derive an expression for CTL-mediated killing,

$$E + T \underset{k_{-1}}{\overset{k_1}{\rightleftharpoons}} ET \overset{k_2}{\rightarrow} E + T^*, \tag{3}$$

where k_1 and k_{-1} are the rates of conjugate formation and dissociation; k_2 is the killing rate; and E, T, ET, and T^* represent free cognate CTLs, free target cells, CTL-target conjugates, and dead targets, respectively. In this model, the killing rate k_2 is assumed to be exponentially distributed, which is different from a fixed time required to kill a target t_D used in our CPM simulations.

In brief, they used a total quasi steady-state approximation (tQSSA) to find that the number of cells killed over a time period Δt is given by

$$\begin{aligned} K_{\text{full}} &= k_2 \Delta t C \\ &= k_2 \Delta t \frac{h + \overline{E} + \overline{T} - \sqrt{\left(h + \overline{E} + \overline{T}\right)^2 - 4\overline{E}\,\overline{T}}}{2}, \end{aligned} \tag{4}$$

where C is the number of conjugates; $\overline{E}$ and $\overline{T}$ are the total number of cognate CTLs and target cells, respectively; k_2 is the killing rate of target cells; and h is the Michaelis constant defined as $(k_2 + k_{-1})/k_1$. Hereafter, this model is referred to as the full QSSA model. Borghans et al. (9) further showed that a simplified expression can be derived by using a Padé approximation of Eq. 4 (hereafter referred to as the "Padé model"):

$$K_{\text{Padé}} = k_2 \Delta t C = \frac{k_2 \Delta t \overline{E}\,\overline{T}}{h + \overline{E} + \overline{T}}. \tag{5}$$

This Padé model can be rearranged to a conventional DS model with a single saturation constant,

$$K_{\text{DS}} = \frac{k' \Delta t \overline{E}\,\overline{T}}{1 + \overline{E}/h + \overline{T}/h}, \tag{6}$$

where $k' = k_2/h$. This function is known in ecology as the "Beddington functional response" (25,26). Note that for $h \rightarrow \infty$, the DS model approaches the classical mass-action model:

$$K_{\text{mass}} = k' \Delta t \overline{E}\,\overline{T}. \tag{7}$$

Thus, k' in Eq. 6 is the mass-action killing rate.

As expected from both the full QSSA and the DS models, our monogamous killing simulations show that the number of cells killed saturates to a similar extent when we increase target cell or CTL densities (Fig. 3, *symbols*). Fitting the DS model to our simulations, we find that it describes the data fairly well (sum of squared residuals (SSR) $= 1.4 \times 10^6$; see Table 3 for best fit parameters; Fig. 3 *A*, *lines*). Because the DS approximation poorly describes the data at high densities, whereas we expected the simulation model to be described well by the total Michaelis-Menten model, we examined whether the full QSSA (Eq. 4) describes the data better at high cell densities. Indeed, the full QSSA model describes the simulation data well at all CTL/target numbers (SSR $= 1.07 \times 10^5$; Fig. 3 *B*, *lines*). Because the DS and full QSSA models have the same number of parameters, the lower SSR indicates that the full QSSA provides a better description of the data.

The excellent fit of the full QSSA model suggests that the total Michaelis-Menten model is indeed an appropriate mechanistic description of the monogamous interactions between killers and targets, and that the poor performance of the DS model at high densities is due to the Padé approximation used to derive the functional response (27). Thus, the full QSSA model represents an excellent mechanistic functional response for the monogamous killing regime, yet the DS model performs almost as well as long as cognate cell densities remain sufficiently low.

Joint killing

In our simulations for the joint killing regime, multiple CTLs jointly kill a target cell, as was recently suggested (see the supplementary movies of Caramalho et al. (13)). For such joint killing, Merrill (10) also used the Michaelis-Menten analogy and derived a model similar to the Padé model (Eq. 6), allowing multiple CTLs to bind and jointly kill a single target cell. He considered the rate of synapse formation to be proportional to the number of free binding sites on CTLs and target cells, and proposed the dynamics of the number of occupied binding sites on target cells, i.e., synapses (C_b), to be given by

$$\frac{dC_b}{dt} = k_1\left(\overline{E} - C_b\right)\left(n\overline{T} - C_b\right) - (k_{-1} + k_2)C_b, \tag{8}$$

where k_1 and k_{-1} are, respectively, the rates of conjugate formation and dissociation; k_2 is the killing rate; n is the number of binding sites per target cell; and $\overline{E}$ and $\overline{T}$ are, as before, the total number of cognate CTLs and target cells present at time t. Using the tQSSA, Merrill found that for $C_b << n\overline{T}$, the total killing rate, K_{merrill}, is given by a DS function, with a stronger saturation of killing in target cells than in CTLs (hereafter referred to as "Merrill's model")

$$K_{\text{merrill}} = \frac{nk_2\overline{E}\,\overline{T}}{K_m + \overline{E} + n\overline{T}}, \tag{9}$$

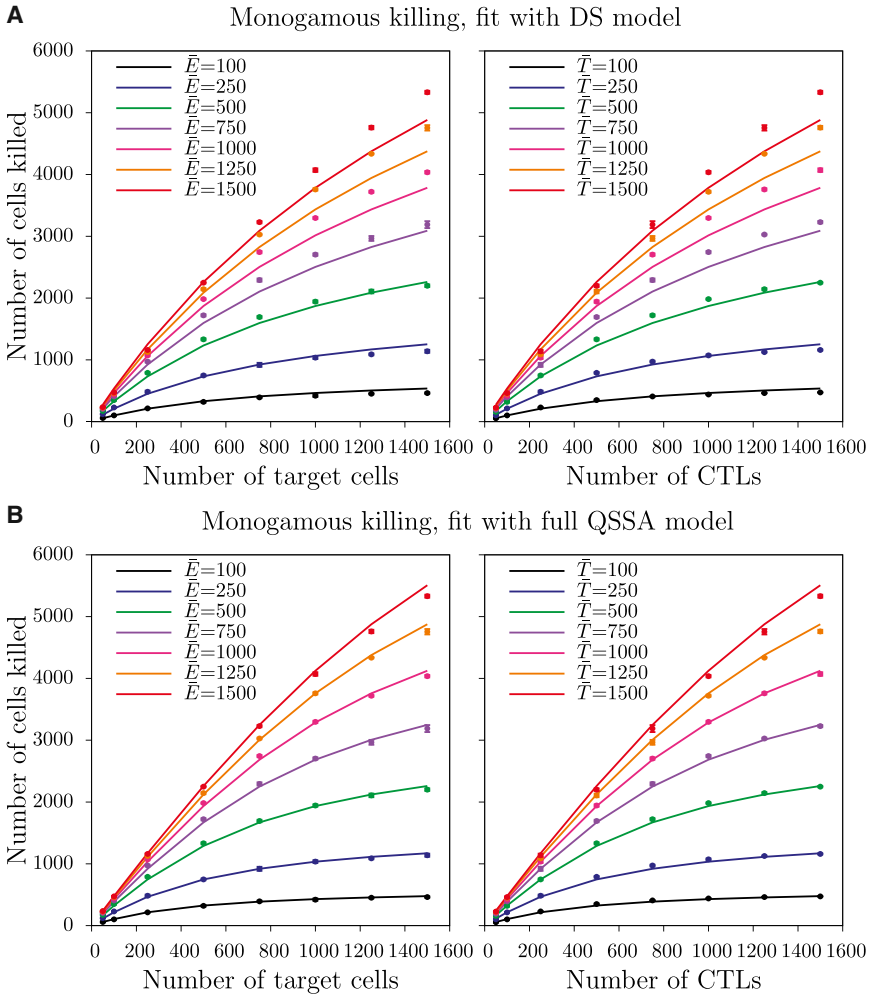

FIGURE 3 Number of target cells killed for monogamous killing. The total number of cells killed over 75 min of simulation as a function of target cell (*left panels*) and CTL (*right panels*) densities for the monogamous killing regime. (*Markers*) Mean of the total number of cells killed over six independent runs. (*Error bars*) Standard deviation. (*Solid lines*) Predictions obtained by fitting the DS model (*A*) and the full QSSA (*B*) with the best-fit parameters. Parameter estimates: $k = 1.808 \times 10^{-4}$ cells^{-1} min^{-1} and $h = 571$ cells for the DS model, and $k = 8.113 \times 10^{-2}$ cells^{-1} min^{-1} and $h = 391$ cells for the full QSSA model. To see this figure in color, go online.

where $K_m = (k_2 + k_{-1})/k_1$. The above equation can be rearranged into a conventional DS model with two different saturation constants,

$$K_{\text{merrill}} = \frac{k'\overline{E}\,\overline{T}}{1 + \overline{E}/h_E + \overline{T}/h_T}, \tag{10}$$

where $k' = nk_2/K_m$ is a mass-action killing rate, $h_E = K_m$ is the saturation constant in CTL, and $h_T = K_m/n$ is the saturation constant in targets.

To identify the conditions for which Merrill's model is valid, we attempt to deduce it from a full cell-based model.

TABLE 3 Best fit parameters (95% confidence intervals shown in the parentheses) of the DS model for different killing regimes

Regime	k' (cells^{-1} min^{-1})	h_E (cells)	h_T (cells)
Monogamous	$1.808\ (\pm 0.143) \times 10^{-4}$	571 (±68)	571 (±68)
Joint	$1.845\ (\pm 0.40) \times 10^{-4}$	2051 (±144)	458 (±15)
Simultaneous	$1.812\ (\pm 0.81) \times 10^{-4}$	523 (±36)	2979 (±561)
Mixed	$1.735\ (\pm 0.047) \times 10^{-4}$	1945 (±131)	1945 (±131)

In joint killing, multiple CTLs sequentially bind to target cells, and the transitions that can occur for this case are given by the following reaction scheme,

$$\begin{aligned} E + T &\underset{k_{-1}}{\overset{nk_1}{\rightleftharpoons}} E_1T \xrightarrow{k_2} E + T^*, \\ E_1T + E &\underset{2k_{-1}}{\overset{(n-1)k_1}{\rightleftharpoons}} E_2T \xrightarrow{2k_2} 2E + T^*, \\ &\vdots \\ E_{n-1}T + E &\underset{nk_{-1}}{\overset{k_1}{\rightleftharpoons}} E_nT \xrightarrow{nk_2} nE + T^*, \end{aligned} \tag{11}$$

where k_1 and k_{-1} are the rates of conjugate formation and dissociation, k_2 is the killing rate, and E, T, and T^* represent the free cognate CTLs, the free target cells, and the dead targets, respectively. For conditions limited by synapse formation rather than limited by encounters between CTLs and target cells, the conjugates E_1T form at a rate nk_1. Similarly, because conjugates E_nT have n synapses, they can dissociate at a rate nk_{-1} to give rise to a conjugate $E_{n-1}T$ and a free CTL. Consistent with Merrill's model, we consider CTLs in conjugates E_nT to act independently and together kill

the target cell in E_nT at a rate nk_2. The dynamics of the conjugates are thus given by

$$\begin{aligned}
\frac{dC_1}{dt} &= nk_1\overbrace{\left(\overline{E}-\sum_{i=1}^{n}iC_i\right)}^{\text{free CTLs}}\overbrace{\left(\overline{T}-\sum_{i=1}^{n}C_i\right)}^{\text{free targets}}-(k_2+k_{-1})C_1\\
&\quad-(n-1)k_1C_1\left(\overline{E}-\sum_{i=1}^{n}iC_i\right)+2k_{-1}C_2\,,\\
\frac{dC_2}{dt} &= (n-1)k_1C_1\left(\overline{E}-\sum_{i=1}^{n}iC_i\right)-2k_2C_2-2k_{-1}C_2\\
&\quad-(n-2)k_1C_2\left(\overline{E}-\sum_{i=1}^{n}iC_i\right)+3k_{-1}C_3\,,\\
&\vdots\quad\vdots\\
\frac{dC_n}{dt} &= k_1C_{n-1}\left(\overline{E}-\sum_{i=1}^{n}iC_i\right)-nk_2C_n-nk_{-1}C_n\,,
\end{aligned}\tag{12}$$

where C_1, C_2, and C_n represent the number of conjugates E_1T, E_2T, and E_nT, respectively; $\overline{E}$ and $\overline{T}$ are the total number of CTLs and target cells, respectively; and $\sum_{i=1}^{n}iC_i$ and $\sum_{i=1}^{n}C_i$ are the total number of CTLs bound to target cells and the total number of targets bound to at least one CTL, respectively.

The total number of synapses C_b equals the number of CTLs in conjugates, i.e., $\sum_{i=1}^{n}iC_i$. Therefore, the dynamics of synapses is given by

$$\begin{aligned}
\frac{dC_b}{dt} &= nk_1\left(\overline{E}-\sum_{i=1}^{n}iC_i\right)\left(\overline{T}-\sum_{i=1}^{n}C_i\right)-(k_2+k_{-1})C_1\\
&\quad-(n-1)k_1C_1\left(\overline{E}-\sum_{i=1}^{n}iC_i\right)+2k_{-1}C_2\\
&\quad+2\left((n-1)k_1C_1\left(\overline{E}-\sum_{i=1}^{n}iC_i\right)-2k_2C_2\right.\\
&\quad\left.-2k_{-1}C_2-(n-2)k_1C_2\left(\overline{E}-\sum_{i=1}^{n}iC_i\right)+3k_{-1}C_3\right)\\
&\quad+\ldots+n\left(\left(k_1C_{n-1}\overline{E}-\sum_{i=1}^{n}iC_i\right)-nk_2C_n-nk_{-1}C_n\right).
\end{aligned}\tag{13}$$

Replacing $\sum_{i=1}^{n}iC_i$ with C_b and rearranging, we get

$$\begin{aligned}
\frac{dC_b}{dt} &= k_1\left(\overline{E}-C_b\right)\left(n\overline{T}-C_b\right)-(k_2+k_{-1})C_b\\
&\quad-k_2\sum_{i=2}^{n}\left(i^2-i\right)C_i\,,
\end{aligned}\tag{14}$$

which has an additional term $-k_2\sum_{i=2}^{n}(i^2-i)C_i$ compared to Merrill's equation (Eq. 8) for the dynamics of the synapses. Thus, unless $C_i \to 0\,\forall\, i \geq 2$, this model cannot be written entirely in terms of C_b. Surprisingly, Merrill's equation can be deduced from the full model if the killing rate of the target cell in E_nT conjugates is the same as that in a conjugate E_1T (see the Supporting Material).

We simulated the joint killing regime (see Movie S2) by allowing target cells to be in conjugate with multiple CTLs at the same time and by increasing the speed at which a target is killed when it is bound to multiple CTLs (see Fig. S4). Interestingly, we found that the number of cells killed saturates as a function of the target cell density, but increases almost linearly with the CTL density (Fig. 4 *A*), which is consistent with Merrill's model (10). To determine whether Merrill's analysis can provide a phenomenological description of our simulation data, we fit the DS model (Eq. 10) and find that this model describes the data quite well (Fig. 4 *A*; see Table 3 for parameters). We find a 4.5-fold difference in the saturation constants, which according to Merrill's model (10) gives an approximate number of binding sites (i.e., maximum number of synapses per cell; see Fig. S2 for distributions of binding sites). The difference in the saturation constants after fitting with the DS model with two different saturation constants can thus help us to distinguish the joint killing from other regimes.

Simultaneous killing

Wiedemann et al. (12) experimentally observed that individual CTLs can also simultaneously kill multiple target cells at the same time. Our simulations (see Movie S3 and Fig. S4) for such a simultaneous killing regime show that there is little saturation of CTL killing with target cell density and strong saturation with CTL density (Fig. 4 *B*), i.e., saturation is reversed compared to joint killing. This finding is consistent with the simulations by Graw and Regoes (11), in which the functional response saturates with CTL density only. In their simulations, conjugates of multiple targets and multiple CTLs are allowed, however. But, although multiple CTLs can bind to a target cell, only one is allowed to kill it, i.e., the killing time, t_D, does not decrease with the number of CTLs bound to the target. This implies that the killing regime of Graw and Regoes (11) is similar to our simultaneous killing regime, thus explaining why our results are consistent with theirs.

Next, we examine whether an analytical functional response can be mechanistically derived from a cell-based model. Similar to our analysis for joint killing regime, we consider single CTLs to bind sequentially to m target cells for binding-limited conditions, so the transitions for this case are given by the reaction scheme

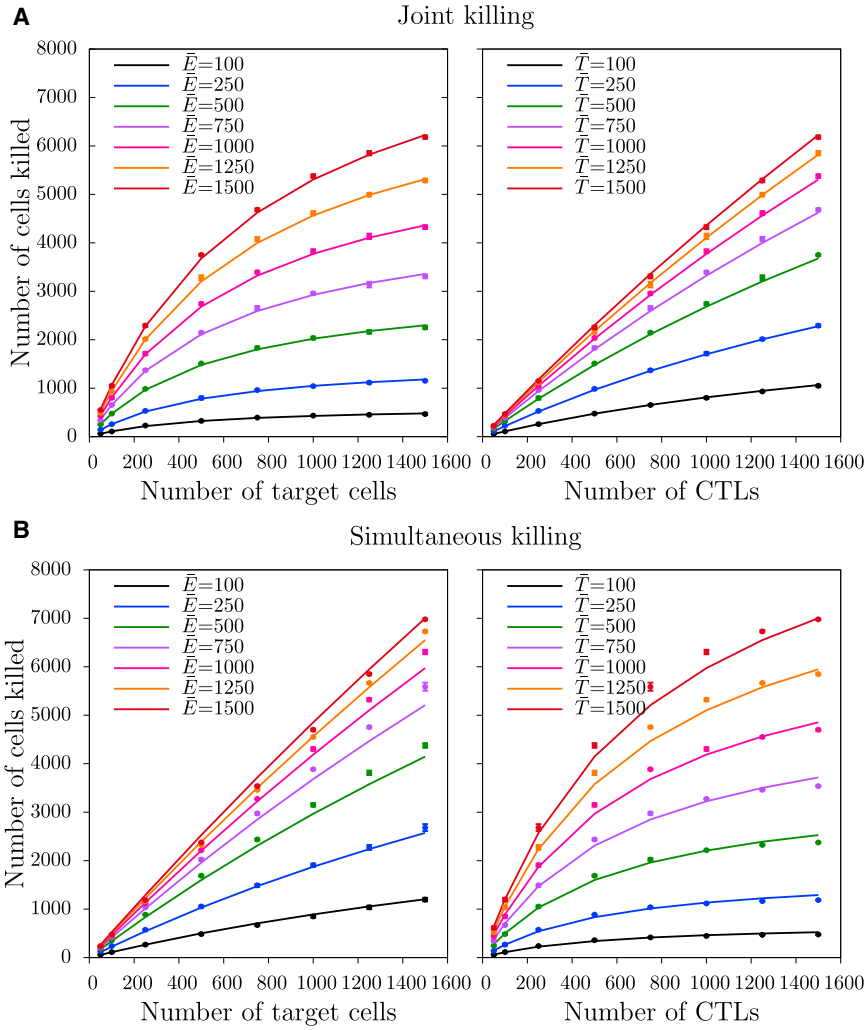

FIGURE 4 The total number of cells killed over 75 min of simulation as a function of target cell (*left panels*) and CTL (*right panels*) densities for (*A*) joint and (*B*) simultaneous killing. (*Markers*) Mean of the total number of cells killed over six independent runs. (*Error bars*) Standard deviation. (*Solid lines*) Predictions of the DS model from Eq. 23 with best-fit parameters (see Table 3). To see this figure in color, go online.

$$
\begin{aligned}
E + T &\underset{k_{-1}}{\overset{mk_1}{\rightleftharpoons}} ET_1 \xrightarrow{k_2} E + T^*,\\
ET_1 + T &\underset{2k_{-1}}{\overset{(m-1)k_1}{\rightleftharpoons}} ET_2 \xrightarrow{2k_2} ET_1 + T^*,\\
&\vdots\\
ET_{m-1} + T &\underset{mk_{-1}}{\overset{k_1}{\rightleftharpoons}} ET_m \xrightarrow{mk_2} ET_{m-1} + T^*,
\end{aligned}
\tag{15}
$$

where k_1 and k_{-1} are the rates of conjugate formation and dissociation, k_2 is the killing rate, and E, T, and T^* represent the free cognate CTLs, the free target cells, and the dead targets, respectively. We consider the target cells in conjugates ET_m to be killed independently by the CTLs. Therefore, the conjugates ET_m are lost when any of the m target cells is killed, i.e., at a rate mk_2. Because CTLs have m binding sites, ET_1 conjugates form at a rate mk_1, and ET_m conjugates dissociate into ET_{m-1} and a free T at a rate mk_{-1}. Therefore, the dynamics of conjugates are given by

$$
\begin{aligned}
\frac{dD_1}{dt} &= mk_1 \overbrace{\left(\overline{E} - \sum_{i=1}^{m} D_i\right)}^{\text{free CTLs}} \overbrace{\left(\overline{T} - \sum_{i=1}^{m} iD_i\right)}^{\text{free targets}} - (k_2 + k_{-1})D_1\\
&\quad - (m-1)k_1 D_1 \left(\overline{T} - \sum_{i=1}^{m} iD_i\right) + 2k_{-1}D_2 + 2k_2 D_2,\\
\frac{dD_2}{dt} &= (m-1)k_1 D_1 \left(\overline{T} - \sum_{i=1}^{m} iD_i\right) - 2k_2 D_2 - 2k_{-1}D_2\\
&\quad - (m-2)k_1 D_2 \left(\overline{T} - \sum_{i=1}^{m} iD_i\right) + 3k_{-1}D_3 + 3k_2 D_3,\\
&\vdots \qquad \vdots\\
\frac{dD_m}{dt} &= k_1 D_{m-1} \left(\overline{T} - \sum_{i=1}^{m} iD_i\right) - mk_2 D_m - mk_{-1}D_m,
\end{aligned}
\tag{16}
$$

where D_1, D_2, and D_m represent the number of ET_1, ET_2, and ET_m conjugates, respectively.

The total number of synapses is

$$C_b = \sum_{i=1}^{m} iD_i.$$

Therefore, the dynamics of synapses is given by

$$\begin{aligned}\frac{dC_b}{dt} =& mk_1\left(\overline{E} - \sum_{i=1}^{m} D_i\right)\left(\overline{T} - \sum_{i=1}^{m} iD_i\right) - (k_2 + k_{-1})D_1 \\ &- (m-1)k_1D_1\left(\overline{T} - \sum_{i=1}^{m} iD_i\right) + 2k_{-1}D_2 + 2k_2D_2 \\ &+ 2\left((m-1)k_1D_1\left(\overline{T} - \sum_{i=1}^{m} iD_i\right) - 2k_2D_2\right. \\ &- 2k_{-1}D_2 - (m-2)k_1D_2\left(\overline{T} - \sum_{i=1}^{m} iD_i\right) + 3k_{-1}D_3 \\ &\left. + 3k_2D_3\right) + \ldots + m\left(k_1D_{m-1}\left(\overline{T} - \sum_{i=1}^{m} iD_i\right)\right. \\ &\left. - mk_2D_m - mk_{-1}D_m\right).\end{aligned} \tag{18}$$

Replacing $\sum_{i=1}^{m} iD_i$ with C_b and rearranging, we get

$$\frac{dC_b}{dt} = k_1\left(m\overline{E} - C_b\right)\left(\overline{T} - C_b\right) - (k_2 + k_{-1})C_b, \tag{19}$$

which is similar to Merrill's equation for joint killing (Eq. 8). Interestingly, we can mechanistically derive Merrill's equation—hence, an analytical functional response—for simultaneous killing from a cell-based model.

Following the approaches of Merrill (10) and Borghans et al. (9), we can formally derive the functional response starting from Eq. 19. Because every synapse induces death of target cells, the rate at which target cells are killed is given by

$$\frac{dT^*}{dt} = k_2C_b. \tag{20}$$

We can find an analytical expression for the killing rate in a similar way as for monogamous killing. Thus, to derive the full solution for the functional response we first make a tQSSA and subsequently simplify using a Padé approximation. The functional response resulting from the full solution is given by (hereafter referred to as the "full QSSA model")

$$\begin{aligned}K_{\text{full}} &= k_2\Delta tC_b \\ &= k_2\Delta t\frac{h + m\overline{E} + \overline{T} - \sqrt{\left(h + m\overline{E} + \overline{T}\right)^2 - 4m\overline{E}\overline{T}}}{2},\end{aligned} \tag{21}$$

where C_b is the total number of synapses, $\overline{E}$ is the total number of cognate CTLs, $\overline{T}$ is the total number of target cells, k_2 is the killing rate of target cells, h is the Michaelis constant defined as $(k_2 + k_{-1})/k_1$, and m is the number of binding sites per CTL.

Using a Padé approximation, the resulting equation for the total number of cells killed over a period Δt becomes

$$K_{\text{Padé}} = \frac{mk_2\Delta t\overline{E}\overline{T}}{K_m + m\overline{E} + \overline{T}}, \tag{22}$$

where $K_m = (k_2 + k_{-1})/k_1$ is the Michaelis constant. Similar to the joint killing scenario, the above equation can be rearranged into a DS model with two different saturation constants, as

$$K_{\text{DS}} = \frac{k'\Delta t\overline{E}\overline{T}}{1 + \overline{E}/h_E + \overline{T}/h_T}, \tag{23}$$

where $k' = mk_2/K_{\text{m}}$, $h_E = K_m/m$, and $h_T = K_m$. This functional response implies an earlier onset of saturation of killing with CTL densities than with target cell densities, which is consistent with our simultaneous killing simulations and is converse to Merrill's model. The ratio of the two saturation constants reflects the number of binding sites, m, on a CTL.

Fitting the DS model of Eq. 23 to the data from our CPM simulations, we find that the DS model describes the data quite well (Fig. 4 *B*). Similar to the fits of the monogamous regime, the fit using the full solution is even better (not shown). As expected, the ratio h_T/h_E provides a good estimate for the number of binding sites on a CTL (i.e., maximum number of synapses per CTL; see Fig. S2 and Fig. S3).

Mixed killing

Finally, we performed simulations (see Movie S4 and Fig. S4) for the mixed killing regime in which a CTL can kill multiple target cells in the same conjugate and target cells can be killed by multiple CTLs. In these simulations, we find that CTL killing saturates approximately at the same target cell and CTL densities (Fig. 5, *symbols*). When compared to the saturation levels in the monogamous killing regime (Fig. 3), the saturation occurs at much higher CTL and target cell densities in the mixed killing regime. This shift in the onset of saturation is because targets and CTLs that are sequestered in complexes can still interact further with other cells. As a result, the time to find a next target cell decreases. Thus, the formation of multicellular conjugates results in an increase in the effective killing capacity of CTLs, and saturation occurs at high cell densities. Similar to the joint killing scenario, we cannot derive an analytical functional response following Merrill's analysis. Nevertheless, because the saturation is symmetric

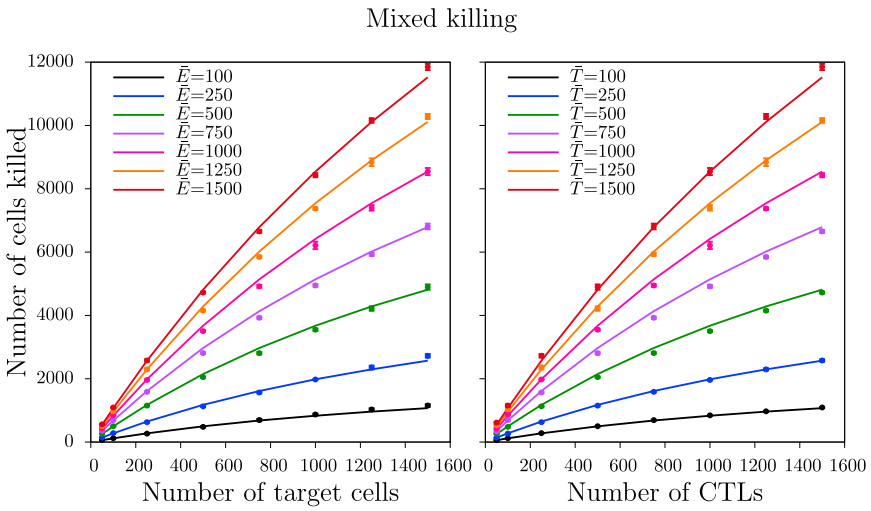

FIGURE 5 The total number of cells killed over 75 min of simulation as a function of target cell (*left panel*) and CTL (*right panel*) densities for mixed killing. (*Markers*) Mean of the total number of cells killed over six independent runs. (*Error bars*) Standard deviation. (*Solid lines*) Predictions of the DS model from Eq. 23 with best-fit parameters (see Table 3). To see this figure in color, go online.

with CTL and target cell densities, it turns out that the phenomenological DS model of Eq. 6 with one saturation constant can fit the data well at all densities examined (Fig. 5; see Table 3 for parameter estimates).

MECHANISTIC INSIGHTS

Because we cannot mechanistically derive the DS model for the joint and mixed killing regimes, we examine the interpretation of its parameters. The generalized DS model with two different saturation constants is given by

$$f(\overline{E},\overline{T}) = \frac{k'\overline{E}\overline{T}}{1+\overline{E}/h_E+\overline{T}/h_T}. \qquad (24)$$

When $\overline{E}\to 0$ and $\overline{T}\to\infty$ (i.e., $\overline{E}/h_E \ll \overline{T}/h_T$), this reduces to $k'h_T\overline{E}$, which is the maximum total CTL killing rate. When $\overline{E}\to\infty$ and $\overline{T}\to 0$ (i.e., $\overline{E}/h_E \gg \overline{T}/h_T$), Eq. 24 reduces to $k'h_E\overline{T}$, which is the maximum rate at which target cells can be killed. At low CTL and target cell numbers, i.e., $\overline{E}\to 0$ and $\overline{T}\to 0$, the per CTL killing rate becomes $k'\overline{E}\overline{T}$. Thus, k' in the DS model (Eq. 24) can be interpreted as a mass-action killing rate. Therefore, even though the DS model cannot be mechanistically derived for all killing regimes, the parameters can be interpreted biologically.

Taken together, our analysis shows that the DS model can be used to interpret the mechanisms of CTL and target cell interactions that underlie cytotoxicity data. If $h_E \approx h_T$, the data point to either monogamous or mixed killing regimes. The asymmetric cases $h_E > h_T$ or $h_E < h_T$, respectively, suggest that joint or simultaneous killing regimes occur.

DISCUSSION

Our aim with this study was to derive a general functional response for target cell killing, which is valid for a wide range of killer and target cell densities. Therefore, we only consider fixed densities, and vary these widely between simulations. Similarly, in the ordinary differential equations (ODEs) we derive the functional response mechanistically by using constant CTL and target cell densities. Thus, our functional response predicts the killing rate at any given density of targets and killers. If in an experimental system these densities change over time (by, e.g., target cell proliferation), one would have to add this to the ODEs that are used to describe the data. If the additional dynamics are fast, this could invalidate the QSSA, and one would have to study the full dynamics of CTL-target interactions.

By simulating CTL killing in an in silico environment resembling T cell areas of lymphoid tissues, we have shown that the number of target cells killed per unit of time is expected to approach a maximum value, i.e., saturates when the density of target cells or that of CTLs becomes large. In asymmetric killing regimes—where either one CTL kills many targets, or where one target is killed by many CTLs—the saturation is also asymmetric (see Table 3). We have generalized a mechanistic function with just one saturation constant into a semimechanistic functional response with two saturation constants, one for the CTLs and another for the target cells.

Whether or not a CTL can jointly kill multiple target cells, and how this affects the time to kill target cells in such multicellular conjugates is not known, and probably depends on factors such as the kind of target cell, its peptide-MHC density, and its presentation of costimulatory molecules. We have studied the simplest cases where one CTL can kill multiple target cells, or a target cell is killed by multiple CTLs in the most efficient way. Because our goal is to use the artificial data for the fitting of mathematical models rather than to give detailed predictions, we here used two-dimensional instead of three-dimensional simulations. The number of CTLs and target cells binding to their counterparts, and the search efficiency of CTLs, are

expected to vary between three- and two-dimensional fields. These differences should only result in different absolute values of the saturation constants. However, the nature of the saturation is expected to remain the same, because our mechanistic ODE models confirm this result and do not depend on the dimensionality of the space.

There are some differences between the conditions of our CPM simulations and our derivation of functional responses. First, following Merrill's model (10), functional responses are derived for binding-limited conditions, whereas killing in our simulations is expected to be diffusion-limited at low cell densities and binding-limited at either high CTL or high target cell densities. However, we find that our DS model still describes the simulation data well, because the target cell killing observed in simulations with either many CTLs or many targets largely determine the saturation constants. Finally, in our simulations we use a fixed kill time t_D of 15 min, whereas this time period is assumed to be exponentially distributed while mathematically deriving the functional responses. Therefore, this suggests that our main conclusions are insensitive to the exact underlying distribution of the killing time t_D. This is important because the precise distribution of killing times in vivo is unknown.

The good fits of the DS model to the simulated data implies that it is robust for the above-mentioned differences. Thus, fitting this simple function to experimental data allows one to estimate both the maximum number of targets a CTL can kill per day, i.e., the maximal killing rate, and the relative sizes of its two saturation constants, which reveals information about the interactions between CTLs and target cells. Because the cellular interactions during the killing of target cells are typically unknown, it seems a good approach to fit experimental data with the general DS model with two different saturation constants to determine the interactions underlying the killing. Interestingly, it was recently found that neutrophil killing of bacteria is also well described by a DS model, with a stronger saturation in the neutrophil density than that in the bacterial density (28). Our results therefore suggest that single neutrophils killing several bacteria at the same time (i.e., our simultaneous killing regime) could be the underlying mechanism in these neutrophil killing assays (28).

Our results reconcile conflicting findings of several recent studies. We have shown that the simulation results of Graw and Regoes (11) with saturation only in the CTL density can be understood from their specific killing regime. We showed that the functional response they found can be mechanistically derived. In another study, Ganusov et al. (6) analyzed in vivo cytotoxicity data in spleens of mice (14) and found that a mass-action model describes the CTL-mediated killing best, i.e., there was no evidence for saturation in killing efficiency.

Our results for a realistic killing time of $t_D = 15$ min (12,20) suggest a saturation constant at a cell frequency of ~10% of all cells for monogamous killing, and at a frequency of ~40% for mixed killing. Because the highest CTL frequency for these in vivo data is ~10% (14), there may indeed be very little saturation in the above-mentioned circumstances. Finally, as Ganusov et al. (6) noted, some of the target cells may have encountered a CTL in vivo, but may actually be killed ex vivo after the spleen had been taken out to count cells. In that case, their rapid estimated killing rate reflects the search time rather than the true killing time in the spleen, and search times are not expected to saturate. Taken together, we propose the DS model as a generic model to describe and quantify killer-target cell dynamics. The relative values of the saturation constants can be used to identify the underlying CTL and target cell interactions in cytotoxicity assays.

SUPPORTING MATERIAL

Three equations, four figures, and four movies are available at http://www.biophysj.org/biophysj/supplemental/S0006-3495(14)00218-5.

The authors thank Renske Vroomans, Jorg Calis, Paola Carrillo-Bustamante, Chris van Dorp, and Ioana Niculescu for critical reading of the manuscript, and technical assistance relating to the CPM and Padé approximation.

This study is supported by The Netherlands Organisation for Scientific Research (NWO) grant No. 819-03-009 (to R.J.d.B.) and by NWO grants No. 916-86-080 and No. 864-12-013 (to J.B.B.). This study is also supported by the Virgo Consortium funded by the Dutch government under project No. FES0908, and by the Netherlands Genomics Initiative under project No. 050-060-452.

REFERENCES

1. Boissonnas, A., L. Fetler, …, S. Amigorena. 2007. In vivo imaging of cytotoxic T cell infiltration and elimination of a solid tumor. *J. Exp. Med.* 204:345–356.
2. Dougan, M., and G. Dranoff. 2009. Immune therapy for cancer. *Annu. Rev. Immunol.* 27:83–117.
3. Morgan, R. A., M. E. Dudley, …, S. A. Rosenberg. 2006. Cancer regression in patients after transfer of genetically engineered lymphocytes. *Science.* 314:126–129.
4. Rosenberg, S. A., B. S. Packard, …, D. E. White. 1988. Use of tumor-infiltrating lymphocytes and interleukin-2 in the immunotherapy of patients with metastatic melanoma. A preliminary report. *N. Engl. J. Med.* 319:1676–1680.
5. Budhu, S., J. D. Loike, …, S. C. Silverstein. 2010. $CD8^+$ T cell concentration determines their efficiency in killing cognate antigen-expressing syngeneic mammalian cells in vitro and in mouse tissues. *J. Exp. Med.* 207:223–235.
6. Ganusov, V. V., D. L. Barber, and R. J. de Boer. 2011. Killing of targets by $CD8^+$ T cells in the mouse spleen follows the law of mass action. *PLoS ONE.* 6:e15959.
7. Schmidt, N. W., N. S. Butler, …, J. T. Harty. 2010. Extreme CD8 T cell requirements for anti-malarial liver-stage immunity following immunization with radiation attenuated sporozoites. *PLoS Pathog.* 6:e1000998.
8. Schmidt, N. W., R. L. Podyminogin, …, J. T. Harty. 2008. Memory CD8 T cell responses exceeding a large but definable threshold provide long-term immunity to malaria. *Proc. Natl. Acad. Sci. USA.* 105:14017–14022.

9. Borghans, J. A. M., R. J. de Boer, and L. A. Segel. 1996. Extending the quasi-steady state approximation by changing variables. *Bull. Math. Biol.* 58:43–63.
10. Merrill, S. J. 1982. Foundations of the use of an enzyme-kinetic analogy in cell-mediated cytotoxicity. *Math. Biosci.* 62:219–235.
11. Graw, F., and R. R. Regoes. 2009. Investigating CTL mediated killing with a 3D cellular automaton. *PLoS Comput. Biol.* 5:e1000466.
12. Wiedemann, A., D. Depoil, …, S. Valitutti. 2006. Cytotoxic T lymphocytes kill multiple targets simultaneously via spatiotemporal uncoupling of lytic and stimulatory synapses. *Proc. Natl. Acad. Sci. USA.* 103:10985–10990.
13. Caramalho, Í., M. Faroudi, …, S. Valitutti. 2009. Visualizing CTL/melanoma cell interactions: multiple hits must be delivered for tumor cell annihilation. *J. Cell. Mol. Med.* 13 (9B, 9b):3834–3846.
14. Barber, D. L., E. J. Wherry, and R. Ahmed. 2003. Cutting edge: rapid in vivo killing by memory CD8 T cells. *J. Immunol.* 171:27–31.
15. Glazier, J. A., and F. Graner. 1993. Simulation of the differential adhesion driven rearrangement of biological cells. *Phys. Rev. E Stat. Phys. Plasmas Fluids Relat. Interdiscip. Topics.* 47:2128–2154.
16. Graner, F., and J. A. Glazier. 1992. Simulation of biological cell sorting using a two-dimensional extended Potts model. *Phys. Rev. Lett.* 69:2013–2016.
17. Beltman, J. B., A. F. M. Marée, …, R. J. de Boer. 2007. Lymph node topology dictates T cell migration behavior. *J. Exp. Med.* 204:771–780.
18. Beltman, J. B., A. F. M. Marée, and R. J. de Boer. 2007. Spatial modeling of brief and long interactions between T cells and dendritic cells. *Immunol. Cell Biol.* 85:306–314.
19. Katakai, T., T. Hara, …, A. Shimizu. 2004. Lymph node fibroblastic reticular cells construct the stromal reticulum via contact with lymphocytes. *J. Exp. Med.* 200:783–795.
20. Mempel, T. R., M. J. Pittet, …, U. H. von Andrian. 2006. Regulatory T cells reversibly suppress cytotoxic T cell function independent of effector differentiation. *Immunity.* 25:129–141.
21. Miller, M. J., S. H. Wei, …, M. D. Cahalan. 2002. Two-photon imaging of lymphocyte motility and antigen response in intact lymph node. *Science.* 296:1869–1873.
22. Parkhurst, M. R., and W. M. Saltzman. 1992. Quantification of human neutrophil motility in three-dimensional collagen gels. Effect of collagen concentration. *Biophys. J.* 61:306–315.
23. Mrass, P., H. Takano, …, W. Weninger. 2006. Random migration precedes stable target cell interactions of tumor-infiltrating T cells. *J. Exp. Med.* 203:2749–2761.
24. Sumen, C., T. R. Mempel, …, U. H. von Andrian. 2004. Intravital microscopy: visualizing immunity in context. *Immunity.* 21:315–329.
25. Beddington, J. R. 1975. Mutual interference between parasites or predators and its effect on searching efficiency. *J. Anim. Ecol.* 44:331–340.
26. Huisman, G., and R. J. de Boer. 1997. A formal derivation of the "Beddington" functional response. *J. Theor. Biol.* 185:389–400.
27. Schnell, S., and P. K. Maini. 2000. Enzyme kinetics at high enzyme concentration. *Bull. Math. Biol.* 62:483–499.
28. Malka, R., B. Wolach, …, V. Rom-Kedar. 2012. Evidence for bistable bacteria-neutrophil interaction and its clinical implications. *J. Clin. Investig.* 122:3002–3011.